Medical Engineering and Physics 101 (2022) 103761

Contents lists available at ScienceDirect

Medical Engineering and Physics

journal homepage: www.elsevier.com/locate/medengphy

Magnetic retrieval of prosthetic heart valves for redo-TAVI

Oguz Can Eren [a], Nick Curzen [b,c], Neil W. Bressloff [*,a]

[a] Computational Engineering and Design Group, Faculty of Engineering and Physical Sciences, University of Southampton, Boldrewood Campus, Southampton, Hampshire SO16 7QF, UK
[b] Faculty of Medicine, University of Southampton, UK
[c] Wessex Cardiac Unit, Southampton University Hospitals NHS Trust, E Level North Wing, Southampton SO16 6YD, UK

ARTICLE INFO

Keywords:
Prosthetic heart valves
TAVI
Valve removal
Cardiovascular

ABSTRACT

Bioprosthetic aortic heart valves are known to degenerate within 7–15 years of implantation. Currently, the options for treating a failing valve are (a) redo surgical aortic valve replacement or, increasingly, (b) valve-in-valve transcatheter aortic valve implantation (ViV-TAVI). The ViV-TAVI procedure is referred to as redo-TAVI when the failing valve is a TAVI device. Repeated procedures, such as two or three valve-in-valves, significantly reduce the effective valve flow area, putting a limit on recurrent treatments. With increasing life expectancy and the use of TAVI in younger, lower-risk patients, the demand for multiple replacement procedures will inevitably increase. Against this background, we describe a novel valve system named exchangeable-TAVI (e-TAVI) in which an electromagnetic catheter is used to remove and retrieve a failed exchangeable valve, followed by the immediate deployment of a new valve. The e-TAVI system comprises (i) an exchangeable valve, (ii) a permanent holding member that anchors the exchangeable valve and (iii) a dedicated catheter with electromagnets for removal of the exchangeable valve. Simulations have been performed to determine the forces, frame design and electromagnetic parameters required to crimp and retrieve a 26 mm diameter valve. An optimum configuration was found to comprise a 12 cell self-expanding frame with circular ferromagnetic regions of 1 mm radius and 0.5 mm thickness, along with eight electromagnets of 1 mm radius and 2 mm thickness. A force of 2.87 N and a current of 2.52 A per electromagnet were required to partially crimp the frame to an envelope radius of 11 mm. While this amount of force allowed the frame to be crimped solely through magnetic attraction, re-sheathing of the frame was not possible due to the weaker shear holding force of the magnets. Also, the current was close to the fusing current of the copper wire needed to fit sufficient windings into the available volume. These issues led to the conclusion that, in addition to the magnetic coupling, a mechanical mating between the removal catheter and the exchangeable valve is needed. This would decrease both the force that the electromagnets had to exert during crimping and the current required to generate this force.

1. Introduction

Severe symptomatic aortic stenosis (AS) can be treated either via surgical aortic valve replacement (SAVR) or, increasingly, transcatheter aortic valve implantation (TAVI) [1,2]. While TAVI was initially developed and approved for use in high-risk patients unable to undergo open heart surgery, more recently, it has been approved for use in lower-risk patients as a result of its clinical performance over the years [3], based upon a series of high quality randomised clinical trials demonstrating equivalency of TAVI with surgery in intermediate- and low-risk patients [4–6]. With the increase in the patient pool for TAVI, the number of patients with a bioprosthetic valve (BV) will inevitably continue to increase [7,8].

A long-term disadvantage of BVs is the attritional susceptibility of the leaflets, which have been observed to degenerate and require replacement within 10 to 15 years of implantation [2,9]. While there is still a lack of data on the long term durability of TAVI BVs, medium term data suggest similar durability to that of the SAVR BVs [10–12]. When a BV fails, the two procedural options are: redo surgical replacement with high procedural risk or, the minimally invasive Valve-in-Valve (ViV) TAVI where a second valve is deployed within the failed one. The main disadvantage of this procedure is the decreasing effective orifice area (EOA) within the annulus of the aortic valve, as another layer of prosthetic material must be accommodated within the previous one [13–16].

* Corresponding author.
E-mail address: N.W.Bressloff@soton.ac.uk (N.W. Bressloff).

https://doi.org/10.1016/j.medengphy.2022.103761
Received 27 August 2021; Received in revised form 14 December 2021; Accepted 18 January 2022
Available online 21 January 2022

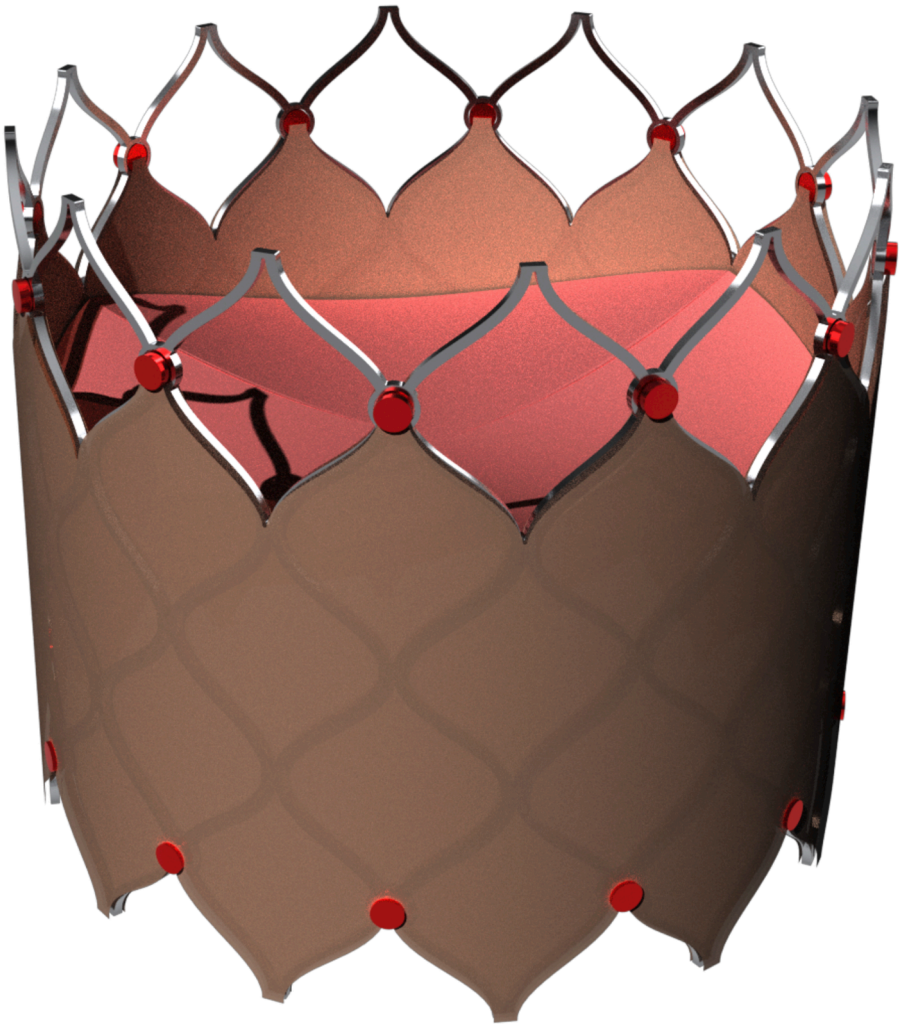

Fig. 1. Concept model of the exchangeable valve frame design for e-TAVI. The ferromagnetic regions lining the circumference of the frame are coloured in red for emphasis. The brown region represents the outer skirt, the pink regions portray the three leaflets, and the frame is coloured grey. (For interpretation of the references to colour in this figure legend, the reader is referred to the web version of this article.)

This "Russian doll" effect, also described as "shrinking annulus", is amplified with each subsequent ViV procedure, putting a clear theoretical limit on recurrent treatment.

The feasibility of a surgical ViV, or redo-TAVI procedure, in terms of clinically satisfactory valvular function, decreases substantially with each new prospective implant due to decreasing EOA. There is currently no satisfactory solution for a clinical challenge that will inevitably become extremely commonplace.

Against this background, the main aim of this work was to design and computationally test the feasibility of a method of crimping a failed TAVI valve in vivo and removing it from the aortic annulus prior to the deployment of a new valve replacement. The key concept in this is that, through the removal of the failed valve, the reduction in EOA can be avoided in successive, minimally invasive valve replacements.

Finite element simulations are commonly utilised in literature for assessing the performance of TAVI devices. Scenarios of device deployment into idealised and patient-specific aortic roots have been successfully simulated to investigate issues such as paravalvular leakage [17], aortic wall damage [18], and radial strength [19,20], to name a few. Further studies verified the accuracy of finite element simulations against in vitro tests of valve frames [19,21–23]. Fluid Structure Interaction studies have also been increasing in number over the years, evaluating the performance of valves under pulsatile flow [24–26]. These, and many other similar publications, contributed greatly towards achieving an accurate methodology for simulating the TAVI procedure, which was used extensively in this work.

2. Methodology

A novel two component valve system, named exchangeable-TAVI (e-TAVI), with a novel dedicated catheter was developed to facilitate the minimally invasive removal and replacement of a prosthetic heart valve. The system comprises:

1. An exchangeable valve with a self-expanding, nitinol frame and a plurality of ferromagnetic regions embedded around the frame (Fig. 1) for attraction with both the electromagnetic catheter and the holding member. The leaflets and skirt are shown for illustrative purposes but were not included in the simulations conducted in the present work.
2. A holding member, shown schematically in Fig. 2, with a plurality of magnetic regions facing radially inward to provide additional anchoring for the exchangeable valve when coupled to the ferromagnetic regions on its frame. The holding member could be surgically implanted or delivered on a catheter. In the surgical case, the initial implantation of the system would need to be accomplished through open heart surgery, but the utility of the holding member becomes apparent in successive valve replacements, which can then

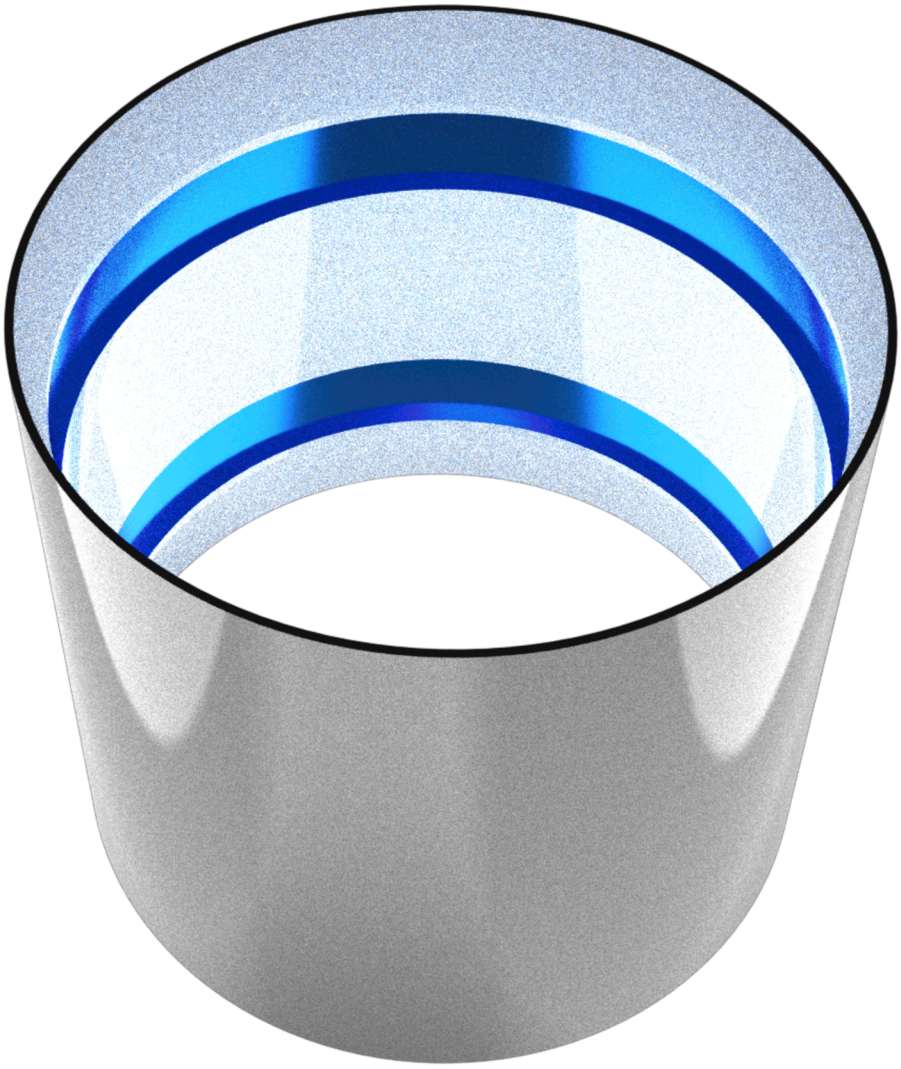

Fig. 2. Concept model of the holding member design for e-TAVI. The magnetic regions are coloured in blue for emphasis, facing radially inward. The exchangeable valve would be deployed within the holding member and the ferromagnetic regions on the frame would be attracted to these magnetic regions. This image is purely conceptual; in reality the member would need a suture ring for surgical implantation or a crimpable frame holding the magnetic regions for delivery via catheter. (For interpretation of the references to colour in this figure legend, the reader is referred to the web version of this article.)

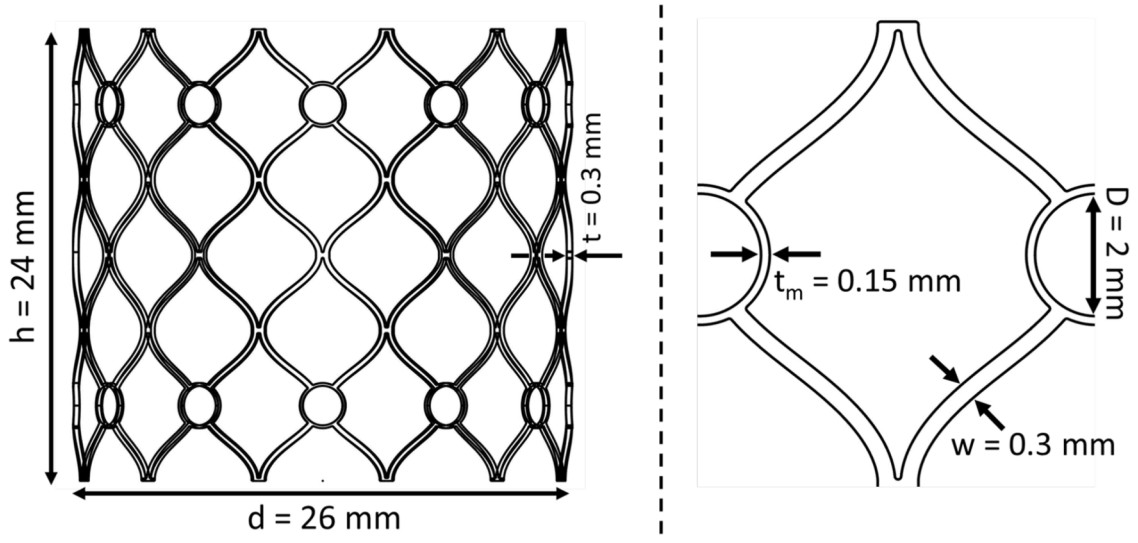

Fig. 3. The dimensions of the exchangeable valve frame. h = valve height, d = valve inner diameter, t = strut thickness, t_m = ferromagnetic region strut thickness, w = strut width, D = ferromagnetic region diameter. All parameters except the ferromagnetic region diameter (D) were kept constant in all simulations.

be done minimally invasively. Through its presence between the aortic wall and the exchangeable valve, the holding member also serves to largely prevent the contact between the exchangeable valve and the aortic wall to minimise tissue build-up around the exchangeable valve.

3. An electromagnetic catheter that can deliver a plurality of electromagnets into the aorta and control the radial movement of the electromagnets such that they can engage with the ferromagnetic regions of the exchangeable valve and pull them inward to crimp the valve frame. For valve retrieval, the catheter also has an openable, tapered sheath that would be withdrawn within the vessel for re-sheathing the valve. Ideally, the catheter would also include a delivery module distal to the electromagnets and the tapered sheath to simultaneously deploy a new exchangeable valve as the previous one is removed.

This article describes a series of experiments that quantified the forces and magnetic parameters required to crimp and re-sheath different exchangeable valve designs in order to identify an optimal configuration and assess the feasibility of the e-TAVI system.

2.1. Exchangeable valve frame design

The frame of the exchangeable valve was based on the cell shape of Medtronic's CoreValve series as it is the most used self-expanding valve on the market [27]. The variable radius of the CoreValve over its height, however, was not included in the design as the purpose of this hourglass shape is to increase the anchoring force of the valve and, in the e-TAVI system, further anchoring is provided by the holding member [28]. Although a shorter nitinol frame would exhibit lower radial strength, the shorter height of the frame compared to that of CoreValve is made possible by the additional anchoring force provided by the holding member. For the e-TAVI scenario, as long as there is sufficient anchoring within the holding member, a lower radial force on the frame is desirable as it makes the removal process easier.

In this study, the height of all designs was 20 mm with strut dimensions of 0.3 mm × 0.3 mm [29,30]. All frame designs included two rings of planar, cylindrical ferromagnetics at the connections between the cells at both ends of the frame as initial experiments showed that the frame could not be adequately crimped through exerting force solely on a single ring of ferromagnets, or on a pair of rings located on the end crowns. Fig. 3 shows the exchangeable valve frame design annotated with dimensions of interest.

Rhino 7 (Robert McNeel and Associates 2020) was used to construct the frame geometries. Explicit finite element analysis was used to simulate the crimping of the frames in ABAQUS CAE/Explicit 2018 [31].

Table 2
Ferromagnetic regions material properties (Neodymium Composite) [33].

Material parameter	Value
Young's modulus	18554 MPa
Poisson's ratio	0.46

The ABAQUS built-in elastic and superelastic property definitions were used to model the behaviour of Nitinol [32]. The material properties of the self-expanding frame are shown in Table 1 [22]. The material properties of the ferromagnetic regions are also shown in Table 2 [33]. The frame was meshed with hexahedral elements (C3D8R), with an edge length of 0.1 mm, following a mesh refinement study, resulting in at least three elements across a frame strut. This resolution agreed with that of finite element analyses of TAVI in literature [19,23,25]. For the design in Fig. 1, this resulted in a mesh with 92,712 elements. Hexahedral elements with reduced integration were used for their lower computational cost and higher tolerance, through the elements being less stiff, to large strain and deformations which occur during crimping simulations. Hour-glassing did not occur throughout the analyses as the mesh resolution was low enough to ensure this [23].

2.2. Modelling magnetic force

In order to simulate the removal of the exchangeable valve using electromagnets, it was necessary to model the distance-dependant nature of magnetic attraction in explicit finite element analysis. The Electromagnetic model for analysing magnetic fields in a static domain is only available in ABAQUS/Standard, so another method of modelling the magnetic force was required in the removal simulations, which were performed on ABAQUS/Explicit due to their dynamic nature [34]. This was accomplished through a dedicated VUAMP subroutine [35]. Sensors were defined on a single node for each ferromagnetic region on the exchangeable frame and on a single node for each electromagnet. These sensors output the global coordinate of each node at every increment. From these coordinates the distance between corresponding ferromagnetic regions and electromagnet pairs were calculated. Given this distance, the magnetic force was calculated through the simplified expression:

$$B = \frac{N \times I \times \mu \times \mu_r}{2} \left(\frac{\frac{D}{2} - z}{D \times \sqrt{R^2 + \left(\frac{D}{2} - z\right)^2}} + \frac{\frac{D}{2} + z}{D \times \sqrt{R^2 + \left(\frac{D}{2} + z\right)^2}} \right) \quad (1)$$

Table 1
Nitinol material model parameters [22].

Material parameter	Symbol	Value
Young's modulus of martensite	E_M	18,554 MPa
Young's modulus of austenite	E_A	40,000 MPa
Poisson's ratio of martensite	ν_M	0.46
Poisson's ratio of austenite	ν_A	0.46
Uniaxial transformation strain	ϵ^L	0.04
Stress at which the transformation begins during loading in tension	σ_{tL}^S	390 MPa
Stress at which the transformation ends during loading in tension	σ_{tL}^E	425 MPa
Stress at which the reverse transformation begins during unloading in tension	σ_{tU}^S	140 MPa
Stress at which the reverse transformation ends during unloading in tension	σ_{tU}^E	135 MPa
Stress at which the transformation begins during loading in compression	σ_{cL}^S	585 MPa
Reference temperature	T_0	37 °C
Slope of the stress versus temperature curve for loading	$\left(\frac{\delta\sigma}{\delta T}\right)_L$	4 MPaT^{-1}
Slope of the stress versus temperature curve for unloading	$\left(\frac{\delta\sigma}{\delta T}\right)_U$	4 MPaT^{-1}

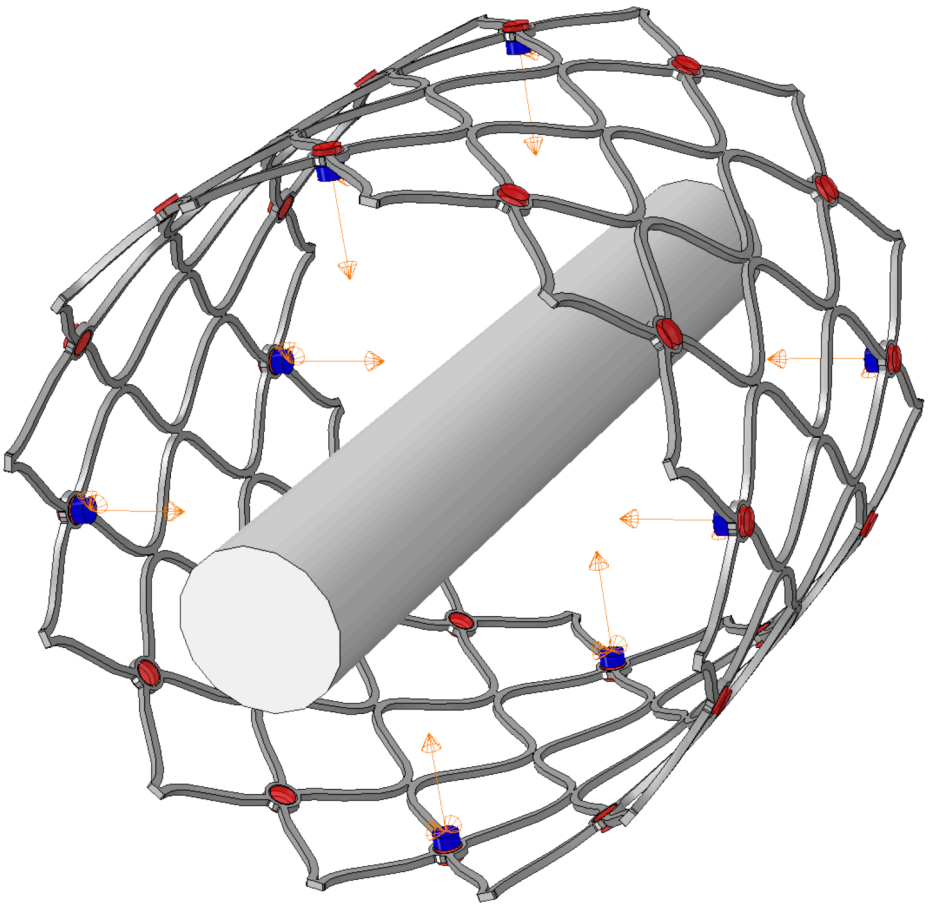

Fig. 4. Assembly for crimping simulations using 4 electromagnets (in blue) per ring in a 12 cell frame. The inner diameter of the frame is 26 mm and the cylinder representing the catheter is 18 Fr (6 mm) in diameter. The orange arrows show the direction of the boundary condition on the electromagnets. The ferromagnetic regions on the frame are in red. (For interpretation of the references to colour in this figure legend, the reader is referred to the web version of this article.)

where N is the number of windings, I is the current through the wire, z is the distance away from the electromagnet pole, D is the thickness of the electromagnet, R is the radius of the electromagnet and μ_r is the relative magnetic permeability of the medium [36]. From this, the force, F, acting on a magnetized area of size A on the same axis is:

$$F = \frac{B^2 A}{2\mu} \tag{2}$$

where μ is the magnetic permeability of the environment [36].

This simplified expression overestimated the magnetic force at separation distances comparable to the radii of the magnets. However, the change in force with respect to the distance was captured correctly. This was verified by a series of magnetostatic simulations where the distance between the electromagnet and ferromagnet was increased from 0.1 mm to 0.45 mm, and the Lorentz force experienced by the ferromagnet in each case was recorded.

It should be noted that Eqs. (1) and (2) were not used to calculate the maximum force exerted by the electromagnet but, instead, were used to determine the force at greater distances, given that at 0.1 mm distance the calculated force agreed with the results of the magnetostatic simulations.

2.3. Crimp shape and envelope diameter

Preliminary experiments had shown that frames adopted a partially crimped, star shaped configuration when applying planar forces at discrete points around the circumference of the frames. Therefore, the first analysis presented here was conducted to determine the crimped shape of the exchangeable valve frames and the diameter of the circular envelopes into which the partially crimped profiles fit. The frame designs were modelled starting from a deployed position without leaflets or skirts. Tie constraints were defined between the frame and the cylindrical ferromagnets. Electromagnets were also modelled as cylinders, with their starting position 0.1 mm away from corresponding ferromagnetic regions on the frame. The magnetic subroutine was used to apply force on the ferromagnetic regions, and a boundary condition was defined on each electromagnet moving them radially inward over the course of the simulation. A cylinder of 6 mm diameter was included in the assembly - representing an 18 Fr catheter - solely to compare the crimped profile with the desired catheter diameter, but there was no contact defined between the catheter and any of the other parts to allow the electromagnets and frame to crimp the furthest distance. An example assembly for this investigation is shown in Fig. 4. The minimum force per electromagnet and the envelope diameter of the resultant crimped frame profile were recorded.

Three exchangeable valve frame designs were considered, differentiated by the number of cells on a single ring of the frame: 12 cells, 9 cells and 8 cells. In terms of commercial valves, the CoreValve series has 12 cells across a single ring and the Portico valve has 9 cells [28,37]. The 8-cell design was investigated for comparison of forces against the 12 cell configuration, even though it lacks the symmetry required to accommodate a tri-leaflet valve. The ferromagnetic regions were placed between each cell on two rings across the height of the frame, resulting in the same number of ferromagnetic regions per ring as the number of cells. The minimum number of electromagnets was set to three as a lower number would not achieve a reduction in size of the envelope for the crimped frame. The maximum was four due to the limited volume in

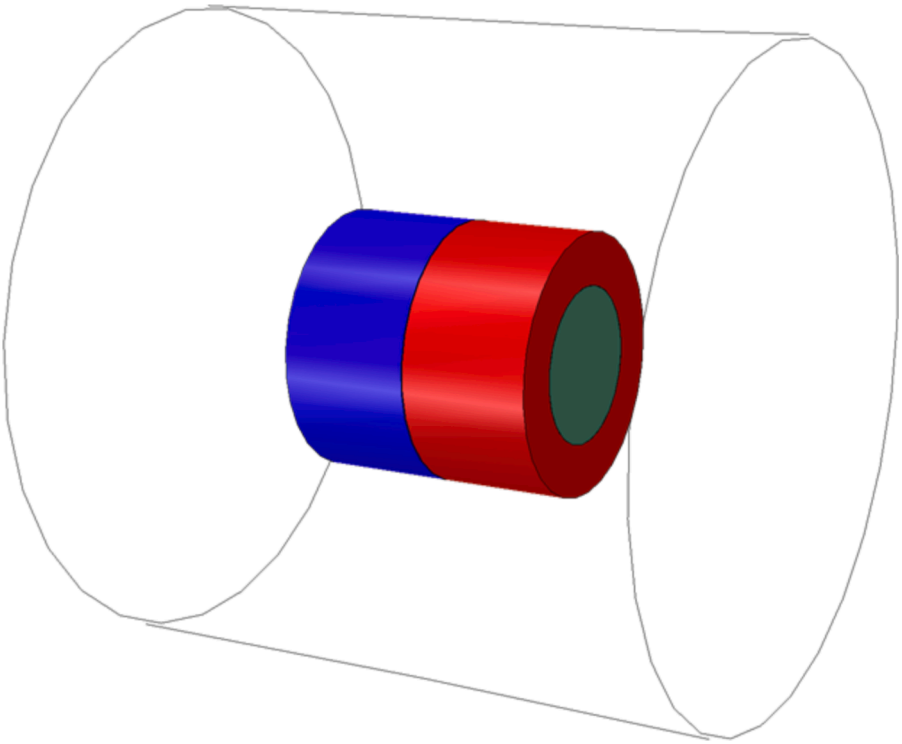

Fig. 5. Assembly of magnetostatic simulations investigating the body current density required to exert the required crimping force. The electromagnet core is in green, the ring representing the windings in red and the ferromagnetic region in blue. The wireframe cylinder surrounding the magnets represents the medium. (For interpretation of the references to colour in this figure legend, the reader is referred to the web version of this article.)

Table 3
Electrical and magnetic material properties used in the magnetostatic finite element simulations.

Material Parameter	Value
Electrical Conductivity (Iron)	10^7 S/m ([38])
Magnetic Permeability (Iron)	6.3×10^{-3} H/m ([39])
Electrical Conductivity (Copper)	5.96×10^7 S/m ([40])
Magnetic Permeability (Copper)	1.256629×10^{-6} H/m ([39])
Electrical Conductivity (Blood)	1.5 S/m ([41])
Magnetic Permeability (Blood)	1.256627×10^{-6} H/m ([42])

the catheter. Additionally, the number of cells on a single ring of the frame had to be divisible by the number of electromagnets for that frame design in order to ensure symmetric crimping. Hence, the frame-electromagnet combinations investigated were:

- 8 cell frame design with 4 electromagnets per ring,
- 9 cell frame design with 3 electromagnets per ring,
- 12 cell frame design with 3 electromagnets per ring,
- 12 cell frame design with 4 electromagnets per ring.

The electromagnet size was kept constant at 0.5 mm radius and 0.5 mm thickness for all four designs in this investigation.

2.4. Ferromagnetic region size and force required to crimp

Having established the minimum forces required to crimp the configurations defined above, the purpose of this analysis was to determine the force per electromagnet required to crimp the 12-cell exchangeable frame design using 4 electromagnets, for different sizes and numbers of ferromagnetic regions on the frame. The same setup to the previous investigation was used with electromagnets moving radially inward and magnetic force being applied to nodes on ferromagnetic regions of the frame through the subroutine. The two scenarios considered both had 24 ferromagnetic regions with a thickness of 0.5 mm, but one had cylindrical ferromagnetic radii of 0.5 mm radius whilst the other had 1 mm radii.

2.5. Electromagnet parameters

Following the identification of force per electromagnet necessary to crimp the exchangeable valve designs, the electromagnet parameters required to exert this force needed to be determined. For the two 12-cell exchangeable frame designs investigated in the previous analysis, a magnetostatic simulation was set up in the Electromagnetic model in Abaqus/Standard. The assembly included a single ferromagnetic region from the exchangeable frame design being investigated and an electromagnet placed 0.1 mm away from the ferromagnet (Fig. 5). The electromagnet was modelled by a cylinder, representing the core, surrounded by a hollow cylinder representing the winding. The material for the core and the ferromagnetic region was defined as iron. The winding was modelled as copper and the medium surrounding the ferromagnet and electromagnet was defined as blood. The electrical and magnetic properties of these materials are listed in Table 3.

An investigation was made regarding the size ratio between the ring and core of the electromagnet and its effect on the maximum pull force while keeping current density constant. The ratio that resulted in the highest force was used in all electromagnet designs.

The electromagnet parameters of interest were electromagnet size (radius and thickness), number of windings (N) and current (I). The size of the electromagnet was constrained at a maximum of 1 mm radius and 2 mm thickness due to the limited volume in the catheter. From this, the following electromagnet sizes (radius, thickness) were included in the investigation:

- 0.5 mm × 0.5 mm

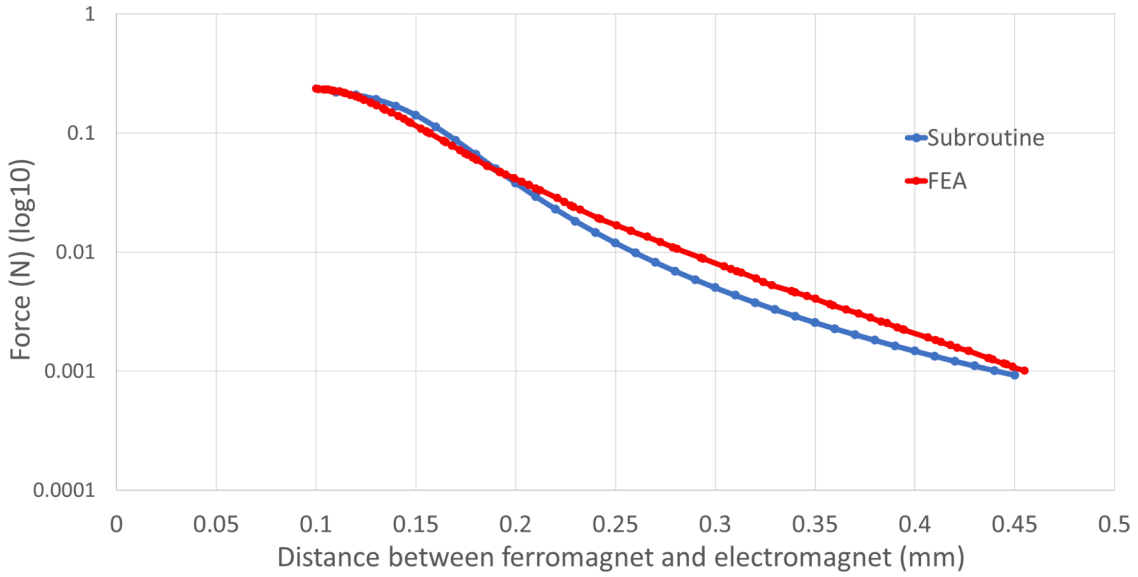

Fig. 6. Comparison between the change in magnetic force between 0.1 mm and 0.45 mm separation predicted by finite element simulations (red) versus the change calculated by the magnetic subroutine (blue). The vertical axis showing the force is in log base 10. (For interpretation of the references to colour in this figure legend, the reader is referred to the web version of this article.)

- 0.5 mm × 1 mm
- 1 mm × 1 mm
- 1 mm × 2 mm

All electromagnet sizes paired with both the small and large ferromagnetic regions sizes from the previous investigation were included in the analysis. The body current density (A/m^3) applied to the ring around the electromagnetic core that resulted in the required force on the ferromagnet was determined for each pair. The determined body current density values were multiplied by the volume of the electromagnet ring representing the windings. This resulted in a total current value, given by current on a single winding multiplied by the number of windings. The number of windings for each electromagnet size was determined by calculating the volume of a single winding, dividing the total volume of the ring by the single winding volume and rounding down to the nearest integer. To calculate the volume of a single winding, the wire radius of this winding had to be determined. For a single electromagnet design, the surface current density (A/mm^2) for wire radii ranging from 0.01 mm to 0.45 mm was analysed to obtain the optimum wire radii.

Finally, the current and number of windings necessary to exert sufficient force was determined for each electromagnet and ferromagnet design to identify the ideal electromagnet size.

2.6. *Re-sheathing*

Following the identification of the optimum exchangeable valve frame design, ferromagnetic regions and electromagnet sizes, the crimping and re-sheathing of this design was simulated. A tapered sheath was modelled with the proximal end to the frame at 24 mm diameter and the distal end at 8 mm. This mimicked a 24 Fr sheath as preliminary investigation showed that the frame design comprising the larger (1 mm) radius ferromagnetic regions could not fit inside a smaller (i.e. 18 Fr) sheath in its crimped shape. Following the partial crimping of the frame through the magnetic subroutine and boundary conditions on the electromagnets, the electromagnets were moved axially, pulling the crimped frame into the tapered sheath. The sheath was modelled as a hard, rigid part. Hard contact definitions were defined between the frame and the sheath with a range of friction coefficients: 0.1, 0.2 and

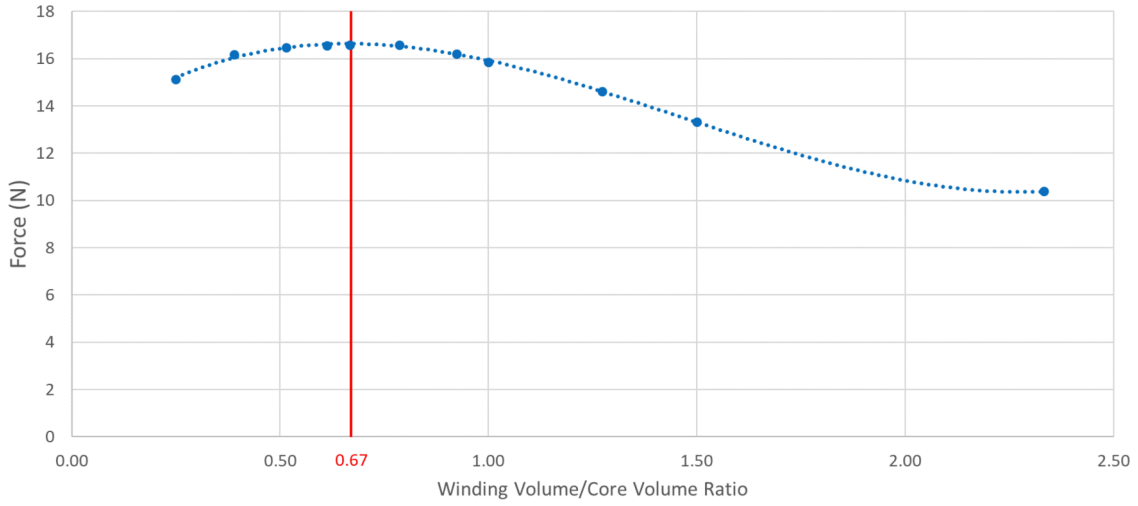

Fig. 7. The relationship between exerted force and core to ring ratio for an electromagnet. The maximum of the curve is labelled with its corresponding core to ring ratio in red. (For interpretation of the references to colour in this figure legend, the reader is referred to the web version of this article.)

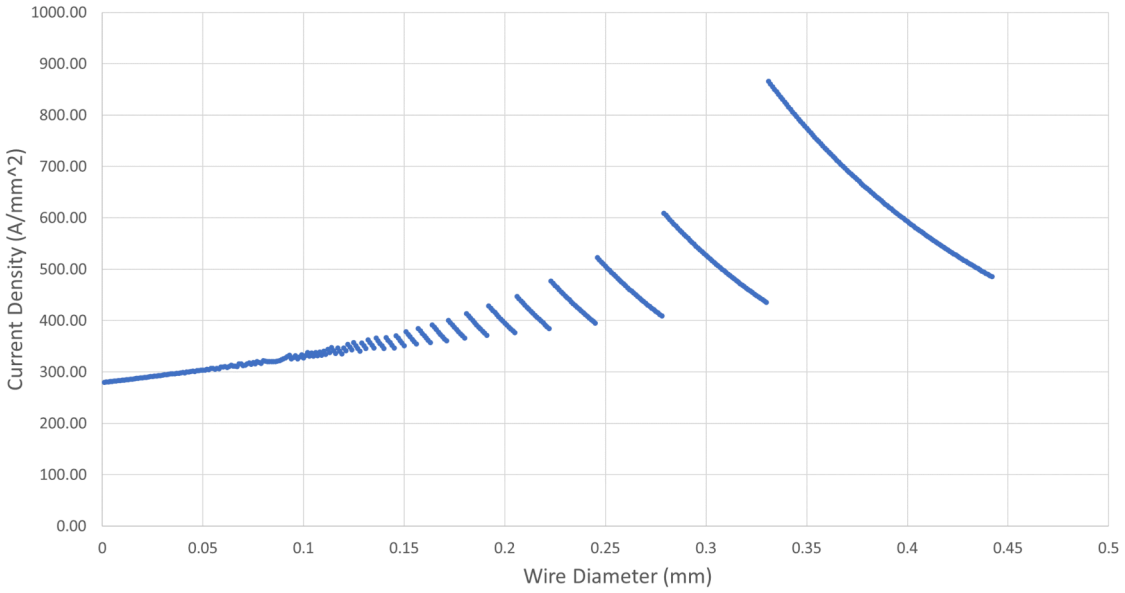

Fig. 8. The relationship between wire radius and surface current density. The surface density tends to increase as wire diameter increases. The discontinuities in the curve occur when the increase in wire diameter causes a decrease in the number of windings that can fit in the given volume.

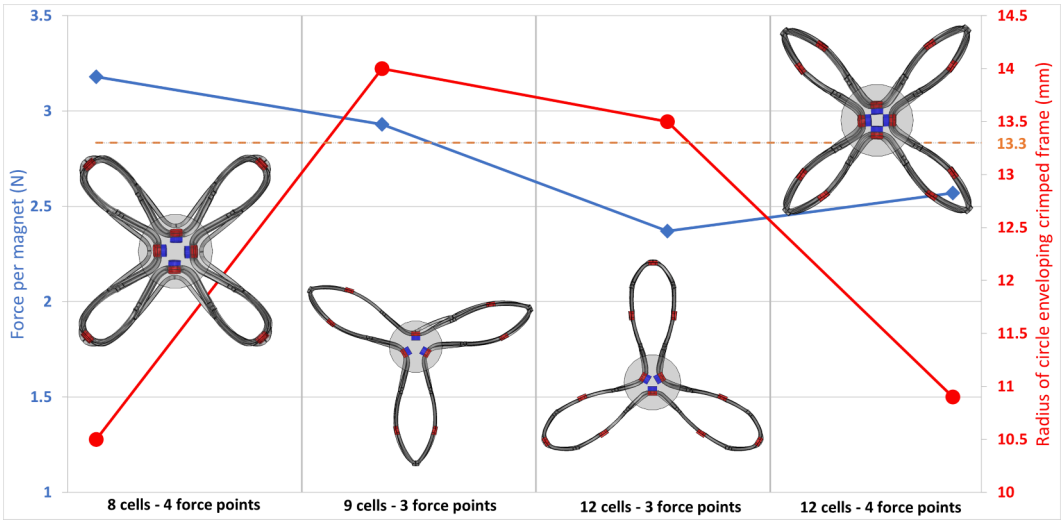

Fig. 9. Left axis (blue): Force (N) per magnet required to crimp (i) an 8 cell frame with 4 electromagnets, (ii) a 9 cell frame with 3 electromagnets, (iii) a 12 cell frame with 3 electromagnets, and (iv) a 12 cell frame with 4 electromagnets. **Right axis (red):** Radius (mm) of circle enveloping the entire final crimped frame for i–iii and iv. A top-down view of the crimped frame for each investigation is shown corresponding with the horizontal axis labels. The dashed orange line shows the 13.3 mm point on the right vertical axis which is the radius of the circle enveloping the frame prior to crimping.

0.3. The friction coefficient range was based on metal-polymer sliding experiments in literature which reported values within that range [43–45]. The different coefficients were observed to have no effect in the success of the re-sheathing.

3. Results

3.1. Magnetic subroutine verification

When the parameters in the subroutine equation (current and number of windings) were set such that the calculated force at 0.1 mm was equal to the Lorentz force at the same distance, the calculated force at higher distance values agreed with the magnetostatic simulations to within 6.15%. The results are shown in Fig. 6. The force calculated at 0.1 mm distance was set as the maximum pull force of the electromagnets because for smaller distance values, the magnetostatic simulations returned lower force values. This lower force was due to the core of the electromagnet and the entire ferromagnet being computed as a single part because of the smaller distance between them, and the resultant force became equivalent to the force exerted by a solenoid on a ferromagnetic cylinder rather than an electromagnet with an iron core.

3.2. Core ratio analysis

It was determined that a 2/3 ratio between the ring and core volume resulted in the maximum force exerted on the ferromagnet for a given current (Fig. 7). Thus, this ratio was upheld in all electromagnet models.

3.3. Wire radii analysis

It was identified that the lower the wire radii, the lower the surface current density (Fig. 8). Since the decrease in current density reduces as

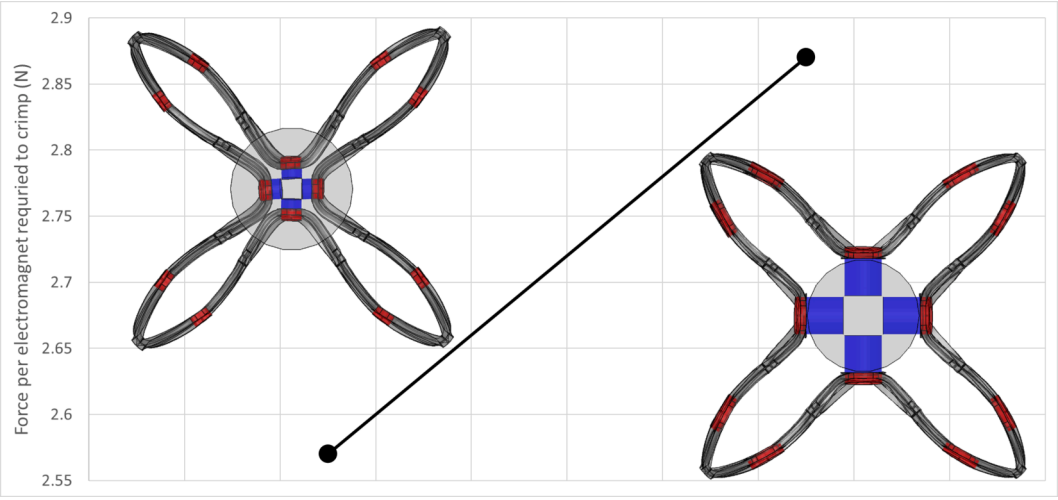

Fig. 10. Force required per electromagnet to crimp exchangeable valve frame designs holding **(left)** smaller ferromagnetic regions (0.5 mm × 0.5 mm) and, **(right)** larger ferromagnetic regions (1 mm × 0.5 mm). The ferromagnets are coloured in red and electromagnets are in blue. The light grey circle in the middle of both frame images represents a 18 Fr catheter. (For interpretation of the references to colour in this figure legend, the reader is referred to the web version of this article.)

Table 4
Electromagnet parameters to exert the threshold force per electromagnet for different combinations of electromagnet and ferromagnetic region sizes. The force requirement to crimp the frame for each ferromagnetic region size is shown in parentheses next to their dimensions. The value labelled density refers to the surface current density of the wire.

		Ferromagnetic region size (Radius × Thickness) (mm)			
		0.5 × 0.5 (2.57 N)		1 × 0.5 (2.87 N)	
Electromagnet Size (Radius × Thickness)(mm)	0.5 × 0.5	Core Radius (mm)	0.3	Core Radius (mm)	0.3
		Number of Windings	14	Number of Windings	14
		Current (A)	26.43	Current (A)	15.36
		Density (A/mm^2)	3365.2	Density (A/mm^2)	1955.3
	0.5 × 1	Core Radius (mm)	0.3	Core Radius (mm)	0.3
		Number of Windings	29	Number of Windings	29
		Current (A)	12.24	Current (A)	6.42
		Density (A/mm^2)	1558.4	Density (A/mm^2)	816.6
	1 × 1	Core Radius (mm)	0.6	Core Radius (mm)	0.6
		Number of Windings	62	Number of Windings	62
		Current (A)	14.76	Current (A)	4.50
		Density (A/mm^2)	1879.3	Density (A/mm^2)	573.0
	1 × 2	Core Radius (mm)	0.6	Core Radius (mm)	0.6
		Number of Windings	125	Number of Windings	125
		Current (A)	8.48	Current (A)	2.52
		Density (A/mm^2)	1079.7	Density (A/mm^2)	320.9

the wire radius is decreased, and that the wire will need to withstand a certain amount of stress as the catheter is manoeuvred through blood vessels, a wire radius of 0.1 mm was chosen to be optimum.

3.4. Crimping force and envelope

The purpose of this investigation was to identify an optimal configuration for the e-TAVI exchangeable valve and electromagnetic system. Fig. 9 shows the results of the crimp shape and envelope investigation. The frame designs were differentiated by the number of cells. As seen in Fig. 9, four electromagnets were required to achieve a meaningful amount of crimping of the frame. For the cases with three electromagnets, the envelope diameter of the crimped frame was higher than that of the initial deployed frame. This is unrealistic in a real setting as the aortic wall would prevent this increase in diameter.

Between the two designs with four electromagnets, the 8-cell design achieved a slightly smaller diameter at 10.5 mm compared to 11 mm for the 12 cell design. However, the 12-cell design required less force per electromagnet to crimp at 2.57 N compared to 3.18 N. Since the force requirement determined the sizes of electromagnets and ferromagnetic regions on the frame, the design requiring the least amount of force while still achieving a decrease in envelope diameter - the 12-cell design with 4 electromagnets - was selected as the optimal configuration.

3.5. Ferromagnetic region size

Fig. 10 shows the results of the ferromagnetic size investigation. As can be seen in Fig. 10, larger ferromagnetic regions resulted in a larger force requirement per electromagnet. This was due to the struts connecting into the ferromagnetic regions being shorter for designs with larger ferromagnetic regions. The shorter struts required more force at one end to deform compared to the longer struts and hence the total force required to crimp increased with ferromagnetic region size.

3.6. Electromagnet parameters

For the required force values identified for each ferromagnetic region size, the electromagnet design parameters that would exert that force on the regions were identified in Table 4. The lowest current requirement was for the pairing between 1 mm × 2 mm electromagnets

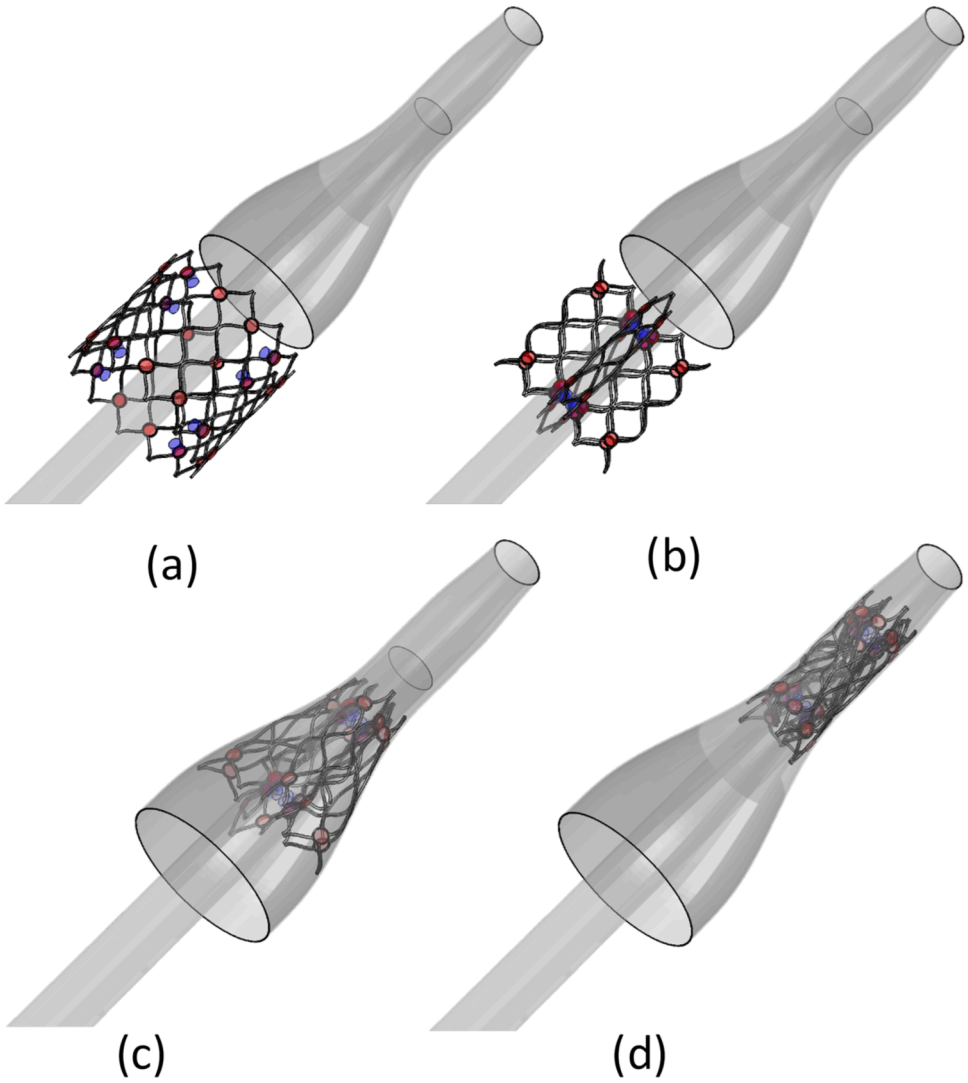

Fig. 11. Series of images showing the partial crimping and re-sheathing of the 12 cell exchangeable frame, holding 1 mm × 0.5 mm ferromagnetic regions, and using 4 electromagnets per ring. (a) Initial deployed position, (b) frame crimped via electromagnets, (c) frame is pulled halfway into the sheath, and (d) frame is fully re-sheathed.

and 1 mm × 0.5 mm ferromagnetic regions. The current requirement in this case was 2.52 A which resulted in a wire current density of 320.9 A/mm^2.

To evaluate the feasibility of transmitting the required current, the fusing surface current density of copper for a wire diameter of 0.1 mm was compared with the experimental current density value. The fusing current depends on the temperature reached in the wire. The widely used equation for calculating this fusing current is based on Preece's experiments in 1888:

$$I = a \times d^{3/2} \tag{3}$$

where I is the current, d is the diameter of the wire, and a is a material dependant constant which is 80.0 A/mm$^{3/2}$ for copper [46]. This equation predicts a fusing current of 2.53 A and a surface current density of 322.1 A/mm^2 for a wire diameter of 0.1 mm. In a lesser cited paper by Schwartz and James in 1905, a piecewise fit to the experimental data of copper fusing current was suggested to be a better fit [47,48]:

$$\begin{aligned} I &= 52.4 \times d^{1.195} \quad d < 0.25 \text{ mm}, \\ I &= 69.9 \times d^{1.403} \quad d > 0.25 \text{ mm}. \end{aligned} \tag{4}$$

This equation predicts a fusing current of 3.34 A and a surface current density of 425.8 A/mm^2 for the same wire diameter.

3.7. Re-sheathing

Fig. 11 shows the results of the re-sheathing simulation. The re-sheathing simulation showed that the 4-pronged shape of the exchangeable valve frame following partial crimping by the electromagnets could be re-sheathed into a 24 Fr sheath, achieving a proof of concept for the removal of an e-TAVI exchangeable valve. However, the axial movement of the frame towards the sheath, or the movement of the sheath towards the frame, could not be achieved through purely magnetic attraction between the exchangeable valve frame and the removal catheter. This was due to the weak shear holding force of the electromagnets where the frame would be detached from the electromagnets and spring back into a fully deployed state as it made contact with the sheath. The full re-sheathing was achieved by defining a tie constraint between the electromagnets and ferromagnetic regions.

4. Discussion

With the growing number of patients likely to need multiple redo valve replacements, and the decreasing feasibility of current minimally invasive redo procedures with each new implant, we aimed to design and computationally test the feasibility of a method of crimping a failed

TAVI valve in vivo and removing it from the aortic annulus prior to the deployment of a new valve replacement. To achieve this, we described a novel valve system named exchangeable-TAVI (e-TAVI) in which an electromagnetic catheter is used to remove and retrieve a failed exchangeable valve, followed by the immediate deployment of a new valve. The system comprised (i) an exchangeable valve, (ii) a permanent holding member that anchors the exchangeable valve and (iii) a dedicated catheter with electromagnets for removal of the exchangeable valve. An optimum configuration for this system was found to have a 12 cell exchangeable valve frame with circular ferromagnetic regions of 1 mm radius and 0.5 mm thickness, along with eight electromagnets of 1 mm radius and 2 mm thickness.

A comparable valve system was designed as part of the Valve-Xchange project [49]. The design consisted of a two component aortic valve system with mechanical mating and did not include any magnetic materials. No further publications apart from the patent filing were made about the development of this valve platform to date since 2011. Another comparable technology is the removal of inferior vena cava filters which is performed minimally invasively via a catheter [50]. However, there are no known publications that have designed or discussed a valve system such as e-TAVI which uses magnetic force in the anchoring and removal of a TAVI valve.

4.1. Electric current

The electric current required for the e-TAVI system is only slightly lower than the fusing currents for the diameter of copper. This shows that it is theoretically possible to transmit the required force through the electromagnets, but the current required is very close to the failure point of the copper wire. It should be noted that these estimates do not consider the sheathing of the wire or any manner of heat sink, so design improvements such as these on the copper wiring could improve the safety margin [47].

4.2. Re-sheathing

The necessity of defining tie constraints between the electromagnets and the ferromagnets in the re-sheathing simulations indicates that a further physical mechanism to attach the frame to the removal catheter is needed to realise the e-TAVI concept. In such a scenario, the attraction between the electromagnets and ferromagnetic regions would be used to achieve alignment and coupling to said physical mechanism on the catheter. Through this physical coupling, the exchangeable valve frame would be crimped and re-sheathed. The coupling would also exert much of the force required for crimping the frame and thus a weaker magnetic attraction between the electromagnets and ferromagnets could be tolerated, decreasing the required current.

4.3. Limitations

The lack of leaflets and skirt in the exchangeable valve model represents one of the limitations in this study. While the effect of including the leaflets in a TAVI deployment simulation were found to be minimal by Bailey et al., in the removal investigation here, the space taken up by the leaflets could increase the minimum feasible crimp diameter [30]. The skirt could also have some effect on the radial strength of the frame and hence require a larger amount of force per electromagnet to crimp. Future work will include the skirt and leaflets to further verify the e-TAVI concept.

The mechanism of the removal catheter was also not considered for this study, particularly the method of radially moving the electromagnets to make contact with the frame and then translating inwards for crimping and retrieval. Also, the method of deploying a tapered sheath that can then be pulled back into the catheter was not explicitly designed.

5. Conclusion

The e-TAVI concept has been developed as a means for removing a degenerated prosthetic valve minimally invasively, in response to the growing number of patients likely to need multiple redo valve replacements through the course of their lives. Investigation of different exchangeable valve frames and magnet configurations has been used to determine an optimal concept comprising a 12-cell frame holding circular ferromagnets of 1 mm radius and 0.5 mm thickness coupled with four electromagnets of 1 mm radius and 2 mm thickness. The force per electromagnet required to partially crimp this configuration was 2.87 N which could be achieved by a current of 2.52 A. While this force was large enough to sufficiently reduce the diameter of the frame from its deployed diameter, an additional holding force was found to be necessary to achieve re-sheathing. This leads to the conclusion that a further mechanical coupling is needed between the catheter and the exchangeable valve frame to allow for complete removal.

Disclosure statement

Curzen is involved in unrestricted research grants from Boston Scientific, HeartFlow and Beck-mann Coulter and receives speaker/consultancy fees from Boston Scientific, HeartFlow and Abbott.

Ethical approval

Not required.

Declaration of Competing Interest

The authors declare that they have no known competing financial interests or personal relationships that could have appeared to influence the work reported in this paper.

Acknowledgements

This work was partially funded by the Engineering & Physical Sciences Research Council. Ethical approval was not required.

References

[1] Ramlawi B, Ramchandani M, Reardon MJ. Surgical approaches to aortic valve replacement and repair–insights and challenges. J Interv Cardiol 2014;9(1):32–6. https://doi.org/10.15420/icr.2011.9.1.32.
[2] Pibarot P, Dumesnil JG. Prosthetic heart valves selection of the optimal prosthesis and long-term management. Circulation 2009;119(7):1034–48. https://doi.org/10.1161/CIRCULATIONAHA.108.778886.
[3] McMorrow R, Kriza C, Urban P, Amenta V, Amaro JAB, Panidis D, et al. Assessing the safety and efficacy of TAVR compared to SAVR in low to intermediate surgical risk patients with aortic valve stenosis: an overview of reviews. Int J Cardiol 2020; 314:43–53. https://doi.org/10.1016/j.ijcard.2020.04.022.
[4] Durko AP, Osnabrugge RL, Kappatein AP. Long-term outlook for transcatheter aortic valve replacement. Trends Cardiovasc Med 2018;28(3):174–83. https://doi.org/10.1016/j.tcm.2017.08.004.
[5] Mariathas M, Rawlins J, Curzen N. Transcatheter aortic valve implantation: where are we now? Future Cardiol 2017;13(6):551–66. https://doi.org/10.2217/fca-2017-0056.
[6] Sarmento-Leite R, de Oliveira GE. Transcatheter aortic valve implantation: where are we in 2020? Int J Cardiovasc Sci 2020;33(5):537–49. https://doi.org/10.36660/ijcs.20200089.
[7] Carroll JD, Mack MJ, Vemulapalli S, Herrmann HC, Gleason TG, Hanzel G, et al. STS-ACC TVT registry of transcatheter aortic valve replacement. J Am Coll Cardiol 2020;76(21):2492–516. https://doi.org/10.1016/j.jacc.2020.09.595.
[8] Ali N, Faour A, Rawlins J, Dawkins S, Appleby CE, MacCarthy P, et al. 'Valve for life': tackling the deficit in transcatheter treatment of heart valve disease in the UK. Open Heart 2021;8(1):e001547. https://doi.org/10.1136/openhrt-2020-001547.
[9] Kostyunin AE, Yuzhalin AE, Rezvova MA, Ovcharenko EA, Glushkova TV, Kutikhin AG. Degeneration of bioprosthetic heart valves: update 2020. J Am Heart Assoc 2020;9(19):e018506. https://doi.org/10.1161/JAHA.120.018506.
[10] Petronio AS, Giannini C. Developments in transcatheter aortic bioprosthesis durability. Expert Rev Cardiovasc Ther 2019;17(12):857–62. https://doi.org/10.1080/14779072.2019.1704624.

[11] Costa G, Criscione E, Todaro D, Tamburino C, Barbanti M. Long-term transcatheter aortic valve durability. J Interv Cardiol 2019;14(2):62–9. https://doi.org/10.15420/icr.2019.4.2.
[12] Blackman DJ, Saraf S, MacCarthy PA, Myat A, Anderson SG, Malkin CJ, Cunnington MS, Somers K, Brennan P. Long-term durability of transcatheter aortic valve proshteses. J Am Coll Cardiol 2019;73(5):537–45. https://doi.org/10.1016/j.jacc.2018.10.078.
[13] Spaziano M, Mylotte D, Theriault-Lauzier P, de Becker O, Sondergaard L, Bosmans J, Debry N, Modine T, Barbanti M, Tamburino C, Sinning J, Grube E, Nickenig G, Mellert F, Bleiziffer S, Lange R, de Varennes B, Lachapelle K, Martucci G, Piazza N. Transcatheter aortic valve implantation versus redo surgery for failing surgical aortic bioprostheses: a multicentre propensity score analysis. EuroIntervention 2017;13(10):1149–56. https://doi.org/10.4244/EIJ-D-16-00303.
[14] Nalluri N, Atti V, Munir AB, Karam B, Patel NJ, Kumar V, et al. Valve in valve transcatheter aortic valve implantation (ViV-TAVI) versus redo-surgical aortic valve replacement (redo-SAVR): a systematic review and meta-analysis. J Interv Cardiol 2018;31(5):661–71. https://doi.org/10.1111/joic.12520.
[15] Silaschi M, Wendler O, Seiffert M, Castro L, Lubos E, Schirmer J, Blankenberg S, Reichenspurner H, Schafer U, Treede H, MacCarthy P, Conradi L. Transcatheter valve-in-valve implantation versus redo surgical aortic valve replacement in patients with failed aortic bioprostheses. Interact Cardiovasc Thorac Surg 2017;24(1):63–70. https://doi.org/10.1093/icvts/ivw300.
[16] Silaschi M, Wendler O, Seiffert M, Castro L, Lubos E, Schirmer J, Blankenberg S, Reichenspurner H, Schafer U, Treede H, MacCarthy P, Conradi L. Transcatheter valve-in-valve implantation versus redo surgical aortic valve replacement in patients with failed aortic bioprostheses. Interact Cardiovasc Thorac Surg 2017;24(1):63–70. https://doi.org/10.1093/icvts/ivw300.
[17] Bianchi M, Marom G, Ghosh RP, Rotman OM, Parikh P, Bluestein D. Patient-specific simulation of transcatheter aortic valve replacement: impact of deployment options on paravalvular leakage. Biomech Model Mechanobiol 2019;18:435–51. https://doi.org/10.1007/s10237-018-1094-8.
[18] Wang Q, Kodali S, Primiano C, Sun W. Simulations of transcatheter aortic valve implantation - implications for aortic root rupture. Biomech Model Mechanobiol 2015;14:29–38. https://doi.org/10.1007/s10237-014-0583-7.
[19] Finotello A, Gorla R, Brambilla N, Bedogni F, Auricchio F, Morganti S. Finite element analysis of transcatheter aortic valve implantation: insights on the modelling of self-expendavle devices. J Mech Behav Biomed Mater 2021;123:104772. https://doi.org/10.1016/j.jmbbm.2021.104772.
[20] Gong X, Pelton AR, Duerig TW, Rebelo N, Perry K. Finite element analysis and experimental evaluation of superelatic nitinol stents. Proceedings of SMST-2003, Monterey, CA. 2003.https://www.nitinol.com/wp-content/uploads/2012/01/002.pdf
[21] Bosi GM, Capelli C, Cheang M, Delahunty N, Mullen M, Taylor AM, et al. A validated computational framework to predict outcomes in TAVI. Sci Rep 2020;10. https://doi.org/10.1038/s41598-020-66899-6.
[22] Nematzadeh F, Sadrnezhaad SK. Effects of material properties on mechanical performance of nitinol stent designed for femoral artery: finite element analysis. Sci Iran. B 2012;19(6):1564–71. https://doi.org/10.1016/j.scient.2012.10.024.
[23] Hopf R, Gessat M, Falk V, Mazza E. Reconstruction of stent induced loading forces on the aortic valve complex. Proceedings of medical image computing and computer assisted intervention society (MICCAI-STENT'12), Nice, France. 2011. p. 104–11.http://campar.in.tum.de/STENT2012/WebHome
[24] Wu MCH, Muchowski HM, Johnson EL, Rajanna MR, Hsu M. Immersogeometric fluid-structure interaction modeling and simulation of transcatheter aortic valve replacement. Comput Methods Appl Mech Eng 2019;357. https://doi.org/10.1016/j.cma.2019.07.025.
[25] Luraghi G, Migliavacca F, Garcia-Gonzalez A, Chiastra C, Rossi A, Cao D, Stefanini G, Matas JFR. On the modeling of patient-specific transcatheter aortic valve replacement: a fluid-structure interaction approach. Cardiovasc Eng Technol 2019;10:437–55. https://doi.org/10.1007/s13239-019-00427-0.
[26] Ghosh RP, Marom G, Bianchi M, Dsouza K, Zietak W, Bluestein D. Numerical evaluation of transcatheter aortic valve performance during heart beating and its post-deployment fluid-structure interaction analysis. Biomech Model Mechanobiol 2020;19:1725–40. https://doi.org/10.1007/s10237-020-01304-9.
[27] Abdel-Wahab M, Jose J, Richardt G. Transfemoral TAVI devices: design overview and clinical outcomes. EuroIntervention 2015;11:W114–8. https://doi.org/10.4244/EIJV11SWA33.
[28] U. F. D. A. FDA. Medtronic corevalve system; medtronic corevalve evolut r system; medtronic corevalve evolut pro system - p130021/s033. 2019. http://www.fda.gov/medical-devices/recently-approved-devices.
[29] Rao RS, Maniar H, Zajarias A. Sapien valve: past, present, and future. Card Interv Today 2015;March/April:35–41.
[30] Bailey J, Curzen N, Bressloff NW. Assessing the impact of including leaflets in the simulation of TAVI deployment into a patient-specific aortic root. Comput Methods Biomech Biomed Engin 2016;19(7):733–44. https://doi.org/10.1080/10255842.2015.1058928.
[31] SIMULIA. Explicit dynamic analysis. 2017a. https://abaqus-docs.mit.edu/2017/English/SIMACAEANLRefMap/simaanl-c-expdynamic.htm.
[32] SIMULIA. Superelasticity. 2017b. https://abaqus-docs.mit.edu/2017/English/SIMACAEMATRefMap/simamat-c-superelasticity.htm#simamat-c-superelasticity.
[33] Grujic A, Talijan N, Stojanovic D, Stajic-Trosic J, Burzic Z, Balanovic L, Aleksic R. Mechanical and magnetic properties of composite materials with polymer matrix. J Min Metall Sect B-Metall 2010;46(1):25–32. https://doi.org/10.2298/JMMB1001025G.
[34] SIMULIA. Electromagnetic analysis procedures. 2017c. https://abaqus-docs.mit.edu/2017/English/SIMACAEANLRefMap/simaanl-c-electricproc.htm.
[35] SIMULIA. Vuamp. 2017d. https://abaqus-docs.mit.edu/2017/English/SIMACAESUBRefMap/simasub-c-vuamp.htm.
[36] Furlani EP. Permanent magnet and electromechanical devices. Academic Press; 2001. https://doi.org/10.1016/B978-0-12-269951-1.X5000-1.
[37] Denegri A, Nietlispach F, Kottwitz J, Suetsch G, Haager P, Rodrigues H, Taramasso M, Obeid S, Maisano F. Real-world procedural and 30-day outcome using the portico transcatheter aortic valve prosthesis: a large single center cohort. Int J Cardiol 2018;253:40–4. https://doi.org/10.1016/j.ijcard.2017.10.101.
[38] Serway RA. Principles of physics. Saunders College Pub.; 1998.
[39] Brown WF. Handbook of chemistry and physics. McGraw-Hill; 1958.
[40] Matula RA. Electrical resistivity of copper, gold, palladium, and silver. J Phys Chem Ref Data 1979;8(4):1147. https://doi.org/10.1063/1.555614.
[41] Abdalla S, Al-ameer SS, Al-Magaishi SH. Electrical properties with relaxation through human blood. Biomicrofluidics 2010;4(3):034101. https://doi.org/10.1063/1.3458908.
[42] Pauling L, Coryell CD. The magnetic properties and structure of hemoglobin, oxyhemoglobin and carbonmonoxyhemoglobin. Proc Natl Acad Sci USA 1936;22(4):210–6. https://doi.org/10.1073/pnas.22.4.210.
[43] Filippova EO, Filippov AV, Shulepov IA. Experimental study of sliding friction for PET track membranes. IOP Conf Ser Mater Sci Eng 2016;125:012020. https://doi.org/10.1088/1757-899X/125/1/012020.
[44] Quaglini V, Dubini P. Friction of polymers sliding on smooth surfaces. Adv Tribol 2011;2011(4):8. https://doi.org/10.1155/2011/178943.
[45] Khoffi F, Khenoussi N, Harzallah O, Drean JY. Mechanical behaviour of polyethylene terephthalate/copper composite filament. Phys Procedia 2011;21:240–5. https://doi.org/10.1016/j.phpro.2011.11.001.
[46] Preece WH. On the heating effects of electric currents. Proc R Soc 1883;36:464–71. https://doi.org/10.1098/rspl.1883.0133.
[47] Babrauskas V, Wichman IS. Fusing of wires by electrical current. Conf Proc - Fire Mater 2011;12:769–80.
[48] Schwartz A, James WHN. Low tension thermal cut-outs. Proc IEEE 1905;35:364–420.110.1049/jiee-1.1905.0060
[49] Vesely I.. Cardiovascular valve assembly. U.S. Patent 2006/0136052, 22 June 2006.
[50] Angel LF, Tapson V, Galgon RE, Restrepo MI, Kaufman J. Systematic review of the use of retrievable inferior vena cava filters. J Vasc Interv Radiol 2011;22(11):1522–30. https://doi.org/10.1016/j.jvir.2011.08.024.